Probing electrochemically induced resistive switching of TiO_2 using SPM techniques

Wanheng Lu,[a] Lai-Mun Wong,[b] Shijie Wang[b] and Kaiyang Zeng[a,*]

a Department of Mechanical Engineering, National University of Singapore,
9 Engineering Drive 1, Singapore 117576.
E-mail: mpezk@nus.edu.sg;
Fax: +65 6779 1459; Tel: +65 6516 6627

b Institute of Materials Research and Engineering (IMRE), Agency for Science, Technology and Research (A*STAR), 2 Fusionopolis Way, Innovis #08-03, Singapore 138634

Abstract

Resistive switching on the nanoscale is an emerging research field and Scanning Probe Microscopy (SPM) is a powerful tool for studies in this area. Under the SPM tip, the electrical field is very high due to the small tip radius on the order of tens of nanometers, and this can enable a range of ionic/electrochemical phenomena during the resistive switching of the materials under the SPM tip. Although the ionic/electrochemical phenomena have long been considered vital for the resistive switching of materials, a few pieces of experimental evidence, as well as the decoupling of the effects of the electrochemical processes at different stages, are still needed. In this work, we applied SPM based techniques to study resistive switching as well as the electrochemical phenomena during the resistive switching of the TiO_2 thin films prepared using Pulse Laser Deposition (PLD). It was found that the reversible or irreversible electrochemical processes initiated at different voltages can promote or degrade the resistive switching behavior of TiO_2. Combined with an electrical cell with environmental control, these electrochemical processes have been shown to require the involvement of moisture; the accumulation of oxygen vacancies, protons, and hydroxyls at the tip/TiO_2 junction may contribute to the promoting effect of the reversible electrochemical process on resistive switching, while the oxygen vacancy ordering and the injection of protons and hydroxyls into the lattice may lead to the irreversible electrochemical process. This work provides a detailed insight into the characteristics, origins, and the effects of the electrochemical phenomena on resistive switching performance, and will provide a further understanding of the electrochemical phenomena in various functional materials.

1. Introduction

Rapid developments in information technology necessitate development of non-volatile memory devices with a high speed, large capacity, and low power consumption. Also, they actuate the miniaturization of the contemporary memory technologies such as the dynamic random access memory (DRAM) and flash memory. As the memory devices are continuously scaled down, they approach their physical and practical limits.[1,2] Many novel memory devices[3–12] have been proposed as the alternatives to the conventional memory technologies, of which resistance random access memory (RRAM) is a promising candidate due to its superior performance compared with other emerging candidates as well as the aforementioned DRAM and flash memory.[1,8,13] RRAM is based on electrically switching the resistance of a metal/insulator/metal (MIM) memory cell between a low resistance state (LRS, or noted as the 'ON' state) and a high resistance state (HRS, or the 'OFF' state). The 'I' in MIM refers to an insulating oxide layer which can be a broad range of transition metal oxides (TMOs).[14–22] In fact, because of the massive number of TMOs demonstrating resistive switching, as well as their wide range of electrical properties that can be modulated by inducing a variety of defects or doping with different elements, the mechanisms underlying resistive switching are still a matter of debate with diverse models.[23] Generally speaking, these models can be categorized into filament based and the interface based mechanisms according to the locations where the resistive switching occurs.[2] The filament based resistive switching primarily results from the formation and rupture of conductive filaments in the insulating oxide layer so that the two metal electrodes can be connected or disconnected,[19] whereas the interface based resistive switching mainly originates from the modification of the interface between oxides and electrodes due to the migration of ions[24,25] and charges.[26,27] There are two points to be noted about resistive switching mechanisms: first, oxygen vacancies, as one type of defect in transition metal oxides, are of great importance for resistive switching due to either their effects in facilitating the filaments or in modulating the interface properties;[2,28,29] second, these two types of resistive switching mechanisms are not absolutely exclusive to each other. In many cases, even for identical materials or systems these two mechanisms may coexist,[30,31] co-function,[32] or convert to each other. This depends on the nature of the oxide layer and the metal electrode,[2] and the oxygen vacancy concentration as well

as the thickness of the oxide layer or the corresponding distance between the two metal electrodes.[33] It is less likely to form/rupture long-length conductive filaments for a large film thickness or electrode distance. Although conductive filaments with lengths up to micrometers have been reported,[34–36] visualization of these filaments has not been available so far.

On the other hand, due to the increasing demand for high density memory devices, there is growing attention that focuses on materials with unique nanostructures, such as nanowires,[17,37–39] nanocrystals,[40,41] and ultra-thin films.[30,42] To explore the properties of those nanostructures, scanning probe microscopy (SPM) based techniques are powerful tools. For example, conductive atomic force microscopy (C-AFM) has been widely utilized to investigate the resistive switching of materials on the nanoscale due to its capacity to visualize the conductive paths.[42–44] The C-AFM tip (generally with a small radius on the order of tens of nanometers) can work as a movable electrode and hence it can be positioned at any specific locations over the sample surface, enabling characterization of the electrical properties of nanoscale structures.[45,46]

Given the small SPM tip radius, the electrical field imposed by the SPM tip on the sample can be very high. Therefore, the ionic motions underneath the SPM tip may be highly intensified. This can cause a broad spectrum of electrochemical phenomena, such as the charging of surface water layers, ionic exchange, and solid state electrochemical reactions, especially when the SPM measurements are performed in the ambient air environment.[47,48] The ionic and electrochemical phenomena on the nanoscale have been verified in recent work to underpin the functionalities of various material systems, for example, Li-ion battery materials.[49–51] In these studies, Electrochemical Strain Microscopy (ESM) is employed to probe electrochemical reactivity and ionic movements in solids down to the 10 nm scale. In ESM, a biased SPM tip concentrates an electrical field in a nanoscale volume of a material near the tip–sample contact, inducing an interfacial electrochemical process at the tip–sample junction and the ionic distribution driven by the concentration or potential gradient. There exists an intrinsic link between the ionic concentration (or the oxidation states of the host cation) and the molar volume of the material. Consequently, the variations of the ionic concentration induced by the biased SPM tip will

result in the fluctuation of the molar volume and thus of surface displacement.[52–56] Using a lock-in technique, the surface displacement can be measured and defined as electrochemical strain, which is directly related to ionic diffusion.[57,58] The relation between the electrochemical strain (or Vegard strain ε) and the ionic concentration change Δn can be denoted as:[55]

$$\varepsilon = \beta \Delta n \quad (1)$$

where β is the Vegard coefficient.

Although these ionic or electrochemical effects have been reported for the nanoionics-based[29] and redox-based[59] RRAM, few studies have been conducted on the ionic and electrochemical phenomena during the resistive switching of transition metal oxides as well as their influences on the resistive switching performance. This has motivated this study on titanium oxide (TiO_2) thin films. TiO_2 based materials have attracted great attention as potential materials for new generation RRAM since the report of the resistive switching cell based on TiO_2 in 2008.[60–64] In this study, we probe the ionic and electrochemical phenomena during the resistive switching processes of TiO^2. In particular, instead of the vertical configuration used in the previous study where a filament based mechanism was dominantly underlying the resistive switching behavior of $TiO^{2,65}$ a planar resistive switching cell[2,29] is configured with the one metal electrode laterally deposited on the TiO_2 surface and the other electrode is the SPM tip. In such a configuration, the distance between the two electrodes can be adjusted by shifting the movable SPM tip. Hence, by combining various SPM-based techniques, including C-AFM, ESM, and using an electrical cell with environment control, electrochemical phenomena during the resistive switching processes of this planar TiO_2 resistive switching cell are studied. This work will provide detailed insights into the characteristics, origins, and the effects of the electrochemical phenomena on the RS behaviour, which will provide a further understanding of the electrochemical phenomena in various functional materials.

In this work, two modes of the ESM technique, i.e., the imaging mode and the voltage spectroscopic mode, were used. During the imaging mode, a high-frequency periodic voltage V_{ac} is applied to the ESM tip to detect the electrochemical strain over the sample surface. To increase the detection

sensitivity, the bias voltage frequencies are stipulated by the mechanical contact resonance of the cantilever and the sample surface. To track the resonant frequency during scanning, the dual amplitude resonance tracking (DART) technique is often employed, in which the cantilever-sample system is driven at two different frequencies around the resonance frequency and the difference between the amplitudes at these two frequencies serves as the feedback to modulate the driving frequency.[66] With this DARTESM imaging mode as well as the damped harmonic oscillator (DHO) fitting, several images can be obtained, i.e., (i) topography; (ii) phase; (iii) amplitude (which is directly related to the ionic distribution and thus defined as the electrochemical strain); (iv) the Q-factor reflecting the mechanical dissipative properties of the cantilever-sample system; and (v) resonance frequency associated with the contact stiffness at the tip–sample contact. According to the DART-ESM principles, the electrochemical phenomena and the associated mechanical properties can be obtained. For example, the decreased ESM amplitude has been observed in a $LiFePO_4$ cathode material due to the extraction of Li ions during the charging process.[67]

For the voltage spectroscopic ESM, short rectangular voltage pulses (B25 ms) with increasing amplitude are applied to the tip, and this can trigger the ionic transport or electrochemical reactions. After each pulse, the ESM responses are detected. Via this approach, ESM responses as a function of the voltage amplitude can be obtained. The opening of the hysteresis loop of ESM responses vs. voltage has been reported and it can be correlated with the extent of the ionic redistribution[57] and the activation of electrochemical reactions.[50,51]

2. Materials and methods

In this work, titanium oxide (TiO_2) thin film samples were deposited on a glass substrate using the Pulsed Laser Deposition (PLD) technique using a TiO_2 target with 99.90 % purity. The deposition parameters were: (i) the laser frequency and energy were 20 Hz and 300 mJ, respectively; (ii) the substrate was maintained at room temperature; (iii) the oxygen partial pressure during the PLD was kept at 1.6×10^{-6} Torr; and (iv) the deposition duration was 30 mins so that the thin film thickness was

estimated to be about 36 nm. A resistive switching cell with TiO_2 thin films and two metal electrodes was configured laterally, which to some extent resembles the MIM structure for practical applications. A comparison between the real MIM structure and the structure used in this study is stated in the ESI.† The resistive switching performance of the lateral cell and electrochemical phenomena during the resistive switching process were studied using Conductive AFM (C-AFM) and Electrochemical Strain Microscopy (ESM), respectively. All experiments were conducted on a commercial SPM system (MPF-3D, Asylum Research, Oxford Instruments, CA, USA) with conductive Pt-coated Si tips (AC240TM, Olympus, Japan, with a spring constant of 2 N m^{-1}, and a tip radius of 15 nm). Fig. 1 schematically shows the sample stack and the measurement setup used in this study. A silver (Ag) thin layer of 10 mm × 1 mm was deposited using conductive silver paste at room temperature. This layer together with the moveable SPM tip acted as the two metal electrodes for the lateral TiO_2 resistive switching cell. The distance between these two electrodes can be modulated via carefully locating the SPM tip on the sample surface. In addition, it should be noted that the direction of the electrical field at the tip–sample junction for C-AFM and ESM is opposite due to their intrinsic differences in the bias application mode. For C-AFM, the bias is applied on the sample surface (i.e., the Ag electrode) with the SPM tip being grounded bias (termed as the 'sample bias'); whereas for ESM, the bias is applied to the SPM tip and the Ag electrode is grounded (labelled as the 'tip bias'). This means that the positive sample bias in C-AFM is identical to the negative tip bias in ESM or vice versa.

Unless specified, all experiments in this work were performed at room temperature and in the ambient air environment with a humidity of ~50 %. Also, in order to explore sample responses in the controlled environments, we employed a closed electrical cell in which the specific atmosphere can be injected during the measurements. The samples were carefully mounted in this closed electrical cell. Two types of atmospheres were used in this study, including synthetic air (21% oxygen, 79% nitrogen, and H_2O < 5 ppm) and argon gas (purity of 99.9999 %, H_2O < 0.02 ppm, oxygen < 0.01 ppm). To effectively apply the environment control, the desired gas was slowly allowed to flow through the cell for at least 2 hours before the SPM measurements and continued flowing during the measurements.

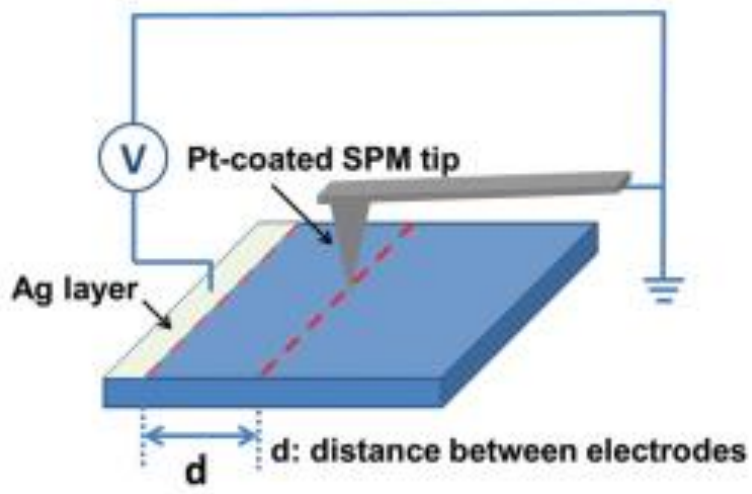

Fig. 1 The schematic of the sample stack and the C-AFM measurements in this work. The Ag layer is deposited on the one end of the TiO_2 film, whereas the Pt coated SPM tip serves as another electrode, and this forms a lateral configured resistive switching cell. By moving the SPM tip, the distance between two electrodes can be tuned. During the C-AFM measurements, voltage is applied on the sample surface via the Ag electrode with the SPM tip grounded, and current passing through this cell is detected.

3. Results and discussion

3.1 Phenomenological observation of electrochemical phenomena during resistive switching of TiO_2

In this work, the resistive switching performance of TiO_2 is analysed using conducting voltage spectroscopic C-AFM on a spatial grid of 8 × 8 points over an area of 3 × 3 mm^2. To avoid the dielectric breakdown of the film, the measurement circuit limits the maximum current to 10 nA. At each point of the 8 × 8 grid, a triangle bias waveform with a frequency of 0.1 Hz is applied and the current passing through the tip–sample junction is measured as a function of the bias waveform to generate the I–V curves. Then all I–V curves obtained at these points are averaged to demonstrate the resistive switching of TiO_2. In addition, the resistive switching behavior of the sample stack is definitely demonstrated to be non-volatile by the current image shown in Fig. S1 (ESI†). As in Fig. S1 (ESI†), the area within the square box (by dashed line) is pre-written to LRS by -6 V. The current outside the box is smaller (with a reading voltage of 2 V), indicating that the LRS can be held when the writing bias (-6 V) is removed.

Fig. 2(a) shows the I–V curve of the TiO2 resistive switching cell with a 3 mm distance between the two metal electrodes. The numbers ‘1’ to ‘4’ indicate the sequence of the bias sweep. The obvious hysteretic I–V loop shown in Fig. 2(a) has demonstrated the resistive switching behavior of the TiO_2

cell. Although in most cases an electroforming process is required to create conductive filaments in the pristine TMO films,[68,69] exceptional examples are also reported where the conductivity of TMO films is good enough so that this electroforming process is not necessary.[32,70] In this work, the resistance between two electrodes (the distance of 3 mm) is measured as ~1 MΩ using a portable multimeter, and the electroforming process is hence absent.

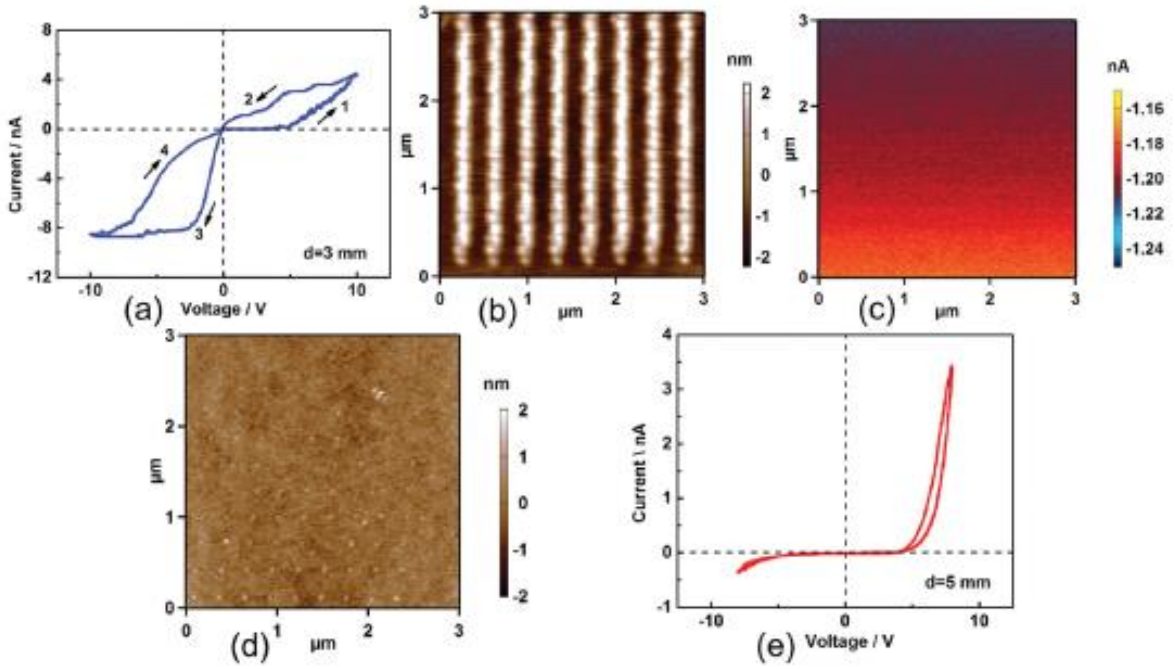

Fig. 2 (a)–(c) C-AFM measurements are conducted on the TiO_2 resistive switching cell with a 3 mm distance between the two electrodes: (a) averaged I–V curve over an 8 × 8 grid, (b) topography, and (c) current image (with a scanning voltage of 1 V) after measuring the I–V curve in this 8 × 8 grid. (d) and (e) C-AFM measurement results when the electrode distance was 5 mm: (d) topography after measuring the I–V curve in a 10 × 10 grid (the Ag electrode is located at the bottom of the image), and (e) averaged I–V curve over this 10 × 10 grid.

After the I–V measurements, the same area is scanned by the C-AFM tip with a reading voltage of 1 V to explore if the applied triangle voltage has changed the topography and the conductivity of the TiO_2 film. Surface deformation after the I–V measurement [as showed in Fig. 2(a)] can be clearly seen as shown in Fig. 2(b). TiO_2 films appear to swell at the locations where the triangle voltage is applied. The swelling is stable and can still be observed even after a long relaxing time up to 12 hours. Surface deformation has been reported to be a good indicator for the electrochemical phenomena,[47] thus we can witness the electrochemical phenomena during resistive switching of TiO_2 from the surface deformation

shown in Fig. 2(b). Fig. 2(c) is the corresponding current image, from which the conductivity variations between the pristine film and swelling have not been detected, indicating that the presence of the electrochemical phenomena has not altered the electrical properties of TiO^2.

After carefully examining the strip swelling in Fig. 2(b), particle-like features can be observed. It is likely that the particles are formed underneath the C-AFM tip and then these particles grow to connect with each other. This particle-like feature can still be easily found in Fig. 2(d), in which the distance between the two metal electrodes has increased to 5 mm. These particles are much smaller compared to those shown in Fig. 2(b), and also their sizes are strongly dependent of the distance between the two electrodes. For example, the particles shown in Fig. 2(d) get smaller from bottom to top where the C-AFM tip moves away from the Ag electrode (on the bottom of the image). It should be noted that even though these particles are very small, they are still much bigger than the tip radius (~15 nm), indicating the possible effects of the water meniscus at the tip–sample junction in the ambient air environment. Fig. 2(e) shows the I–V curve averaged over the points in Fig. 2(d). Compared with the hysteretic I–V curve in Fig. 2(a), the resistive switching performance has been suppressed: only a small I–V loop can be observed. As discussed before, the electrochemical phenomena as surface deformations have presented underneath the SPM tip, this dependence of the surface deformation and resistive switching upon the distance between the electrodes can be explained by the voltage distribution over the measurement set-up shown in Fig. 1. The applied voltage (V) is the sum of potentials at two metal electrode/TiO_2 interfaces and over TiO_2 between two electrodes (the potential of wires and metal electrodes is neglected due to the high conductivity). For the case of the set-up shown in Fig. 1, this can be denoted as:

$$V = V_{Ag} + V_{tip} + V_{TiO2} = I \times (R_{Ag} + R_{TiO2} + R_{tip}) \quad (2)$$

where V_{Ag}, V_{tip}, and V_{TiO2} are the potentials at the Ag/TiO_2 interface, the tip/TiO2 interface and the TiO_2 film between the two metal electrodes, respectively; R_{Ag}, R_{TiO2}, R_{tip} are resistances at the Ag/TiO_2 interface, the tip/TiO_2 interface and the TiO_2 film between the two metal electrodes, respectively; and I is the current.

The potential at the tip/TiO_2 interface can be rewritten as:

$$V_{tip} = \frac{V}{R_{Ag}+R_{TiO2}+R_{tip}} \times R_{tip} \quad (3)$$

when the electrode distance increases, R_{TiO2} will increase; R_{Ag} and R_{tip} should be unchanged due to the intact Ag/TiO_2 interface and the homogeneity of TiO_2. In this case, V_{tip} will decrease as the electrode distance increases. As the potential at the tip–sample junction is the driving force for the localized electrochemical process,[47] the potential decrease will limit the electrochemical processes. Therefore, the particles get smaller when the distance between the electrodes increases. Here, the potential change at the Ag/TiO_2 interface is ignored because the interfacial area (defined as the Ag area of 10 × 1 mm^2 over TiO_2) is much larger than the tip/TiO^2 contact area, and the Ag/TiO_2 interface tends to be ohmic-like contact verified using a multimeter. Thus the potential at the tip/TiO_2 will be affected more significantly. Accordingly, the dependence of resistive switching upon the electrode distance can be seen as the dependence upon the potential at the tip/TiO_2 interface. The main mechanisms underlying resistive switching of transition metal oxides include the filamentary type and the interfacial type.

According to both types of mechanisms, the potential decrease will degrade the resistive switching performance of transition metal oxides as a result of less driving force to move mobile species such as oxygen vacancies to form the conductive filaments or change the interface between the metal electrode and transition metal oxides. In this study, the distances between two electrodes are on the millimeter scale, which is much larger than the electrode distances (in the range of 10–100 nm (ref. 45 and 71)) that is required for the filament-based resistive switching. Also, as mentioned before, the electroforming process, as the defining feature of the filament-based mechanisms,[72] is absent in the TiO2 lateral cell used in this work. All of these have suggested that the interface based mechanisms are behind the resistive switching behavior of the lateral configured TiO_2 resistive switching cell.

3.2 Characterization of electrochemical phenomena during RS of TiO_2

Surface deformations underneath the SPM tip during the I–V measurements have suggested the presence of electrochemical phenomena, specifically, the irreversible electrochemical phenomena. Hence, we further apply the ESM technique together with C-AFM to characterize the electrochemical

phenomena during the resistive switching of TiO_2. Fig. 3 shows the topographic images of TiO_2 after I–V measurements with different amplitudes of voltage. No topographic changes can be observed when the voltages are lower than 6 V, indicating that there is a threshold voltage above which the irreversible electrochemical phenomena can be observed. According to the voltage dependence of the electrochemical processes underneath the SPM tip,[47] before the voltage increases to a critical value that enables the irreversible electrochemical processes, reversible electrochemical processes are likely to proceed. To characterize the reversible electrochemical processes, similar biases like those used in I–V measurements were applied on the sample surfaces and a subsequent ESM technique is used to scan over the same areas.

Fig. 4(a)–(e) show the ESM images obtained after applying a bias with an amplitude of 4 V. As is expected, there are no topographic variations in the height image [Fig. 4(a)], indicating that the irreversible electrochemical process has not been activated under the electrical field of 4 V. However, other images, including amplitude, phase, Q-factor, and frequency images, show variations between the pristine film and the bias written locations (outside vs. within the boxes in Fig. 4), indicating that this 4 V bias has resulted in changes in ionic concentrations and the mechanical properties of the thin films. Specifically, changes in ESM amplitude and resonance frequency are very subtle. Only through carefully looking into these two images, more dark blue points and dark points can be found within the boxes in Fig. 4(b) and (e), respectively. This suggests a slight decrease of the ionic concentration and contact stiffness due to the reversible electrochemical process underneath the SPM tip. Changes in the phase and Q-factor images are much more obvious. The change in the phase is around 30°, and this is much lower than the 180° for the typical piezoelectric/ferroelectric materials. The Q-factor is a measurement of the energy dissipation at the tip–sample junction, and the lower Q-factor at the bias-written locations indicates higher energy dissipation at these points. When the bias is above 4 V, surface deformations and stronger ESM responses can be observed and are shown in Fig. S2 (ESI†).

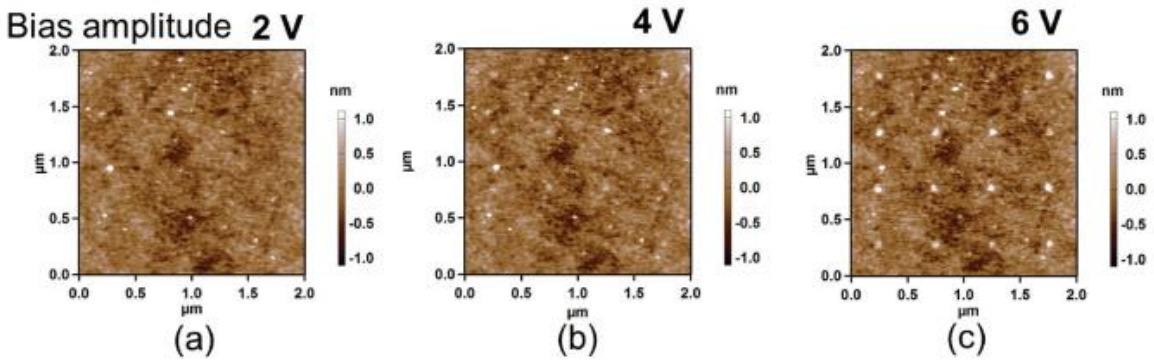

Fig. 3 Topographic images after I–V curve measurements with different bias amplitudes: (a) 2 V, (b) 4 V, and (c) 6 V. When the bias is less than 6 V, the deformation spots are less clear and not all are visible, whereas for the bias larger than 6 V, the deformation spots are clearly visible.

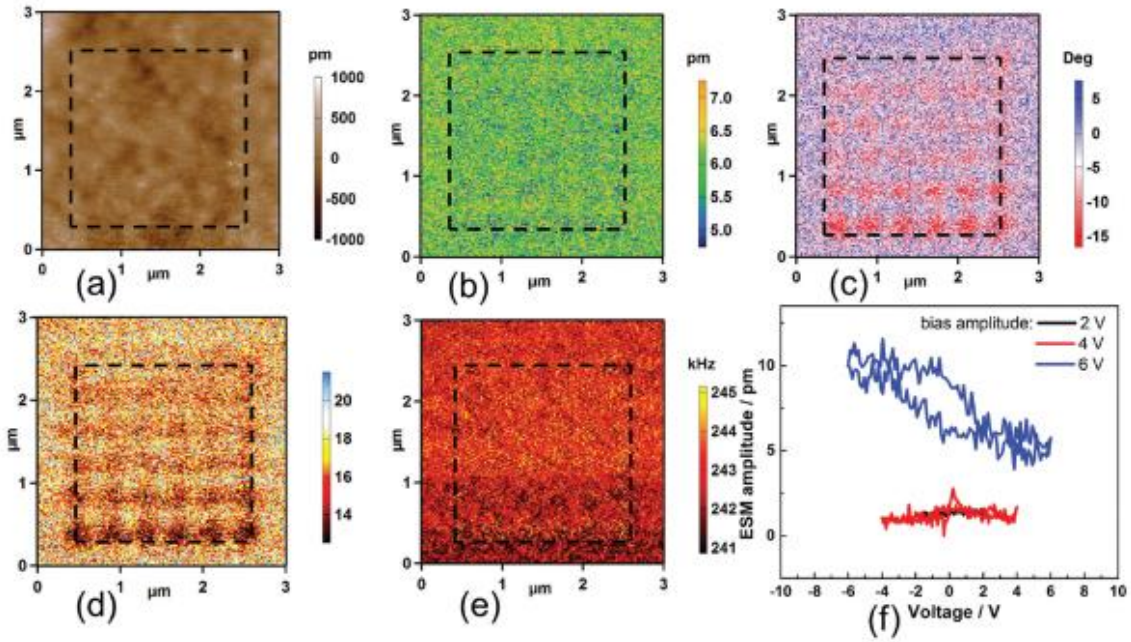

Fig. 4 (a)–(e) ESM images after applying voltage with amplitude of 4 V in a 6 × 6 grid within the dashed box: (a) topography, (b) amplitude, (c) phase, (d) Q-factor, and (e) resonance frequency. (f) ESM amplitude loops as the function of voltage amplitudes.

Furthermore, the ESM response obtained by the voltage spectroscopic ESM as a function of the bias amplitude is shown in Fig. 4(f). The ESM response is measured as a function of slowly changing triangular voltage waveform (0.1 Hz, the same as the one for the C-AFM measurement). In order to minimize the effect of the electrostatic force, the responses are collected when the voltage is off. The opening of the ESM loops apparently depends on the bias amplitude and the environment. As the bias amplitude increases, the ESM loop tends to open and become hysteretic, indicating that the electrochemical activation increases with the bias amplitude. This is in agreement with the voltage

dependence of the electrochemical process shown in Fig. 3. Under the identical electrical field, the ESM loop in ambient air is larger than those in synthetic air and argon gas, and this suppression of the electrochemical process in synthetic air or argon gas will be discussed further in the following section.

The ESM response variations in Fig. 4 strongly indicate the presence of ionic/electrochemical phenomena during the I–V curve measurements. However, the ESM response, in principle, can stem from several reasons such as the piezoelectric effect,[73] the deformation potential effect, the flexoelectric effect, as well as the ionic motion and the associated Vegard strains.[74–77] The centrosymmetric structure of TiO_2 confirmed by the XRD spectrum (Fig. S3, ESI†) can exclude the piezoelectric and hence ferroelectric effects. Moreover, the deformation potential effect and the flexoelectric effect are associated with the fast response of the ionic system to the change of the local electrochemical potential and field gradients, which can contribute to the high frequency ESM response as shown in Fig. 4(a)–(e). However, the slow frequency ESM response in Fig. 4(f) indicates the slow ionic motions. Accordingly, the ESM responses in Fig. 4 have visualized the electrochemical phenomena during the resistive switching of TiO_2.

3.3 Determinative role of electrochemical phenomena in RS of TiO_2

Electrochemical phenomena during the resistive switching of TiO_2, either the reversible or the irreversible, have been observed through the ESM responses and surface deformations. It is therefore necessary to study the origin of these electrochemical phenomena as well as their roles in the resistive switching of TiO_2. For such a purpose, we employed a closed electrical cell filled with the desired gases to conduct the C-AFM and ESM measurements in the controlled environment. Fig. 5(a) and (b) show the surface topographic images after performing I–V measurements similar to experiments shown in Fig. 2(a) in argon gas (moisture & oxygen free) and the synthetic air (moisture free), respectively. The surface deformation disappears in the controlled environments, and this suggests that moisture is a prerequisite in the irreversible electrochemical phenomena. In other words, the surface deformation originates from the moisture involved in the electrochemical phenomena. This is different from the previous finding that oxygen was a required component in the surface deformation in TiO_2.[78] It was

most likely due to the lack of information that allows decoupling the function of oxygen and moisture in the environment. Furthermore, biases similar to those used in I–V measurements are applied and subsequent ESM scanning is performed in the controlled environments. A much smaller ESM response can be observed, and this indicates that in the controlled environments, both the irreversible and the reversible electrochemical processes have been suppressed. This can be verified in Fig. S4 (ESI†), where distinct ESM responses are witnessed in different environments.

Fig. 5(c) shows that the I–V curves obtained in argon gas and synthetic air have no loops. However, when the ambient air is re-injected into the cell, the hysteretic I–V curve reappears. At the same time, the surface deformation can also be clearly seen from Fig. 5(d). This has excluded the possible effects of the SPM tip wearing for the disappearance of the resistive switching in the controlled environments, it also suggests that the resistive switching of the lateral TiO_2 cell is likely the result of the electrochemical processes mediated by the moisture adsorbed at the tip–sample junction.

Fig. 6 shows the I–V curves with different voltage amplitude at two consecutive cycles. Based on the results discussed in Section 3.2, the reversible electrochemical processes occur when the voltage amplitude is less than 6 V (Fig. 3(a) and (b)). The irreversible electrochemical processes are manifested by the surface deformation when voltage is equal to or exceeds 6 V [Fig. 3(c)]. Therefore, Fig. 6 shows the individual effect of the reversible and irreversible electrochemical phenomena on resistive switching. When voltages are less than 6 V, the I–V curves show larger hysteresis at the second cycle than that in the first cycle [Fig. 6(a), (b), (d) and (e)], suggesting an increased effect of the reversible electrochemical phenomena on resistive switching, i.e., the increase of the ON/OFF resistance ratio, RON/ROFF; when the voltage reaches 6 V, the I–V loop becomes smaller at the second cycle compared with that of the first cycle [Fig. 6(c) and (f)], indicating a degraded resistive switching performance as a result of the irreversible electrochemical processes.

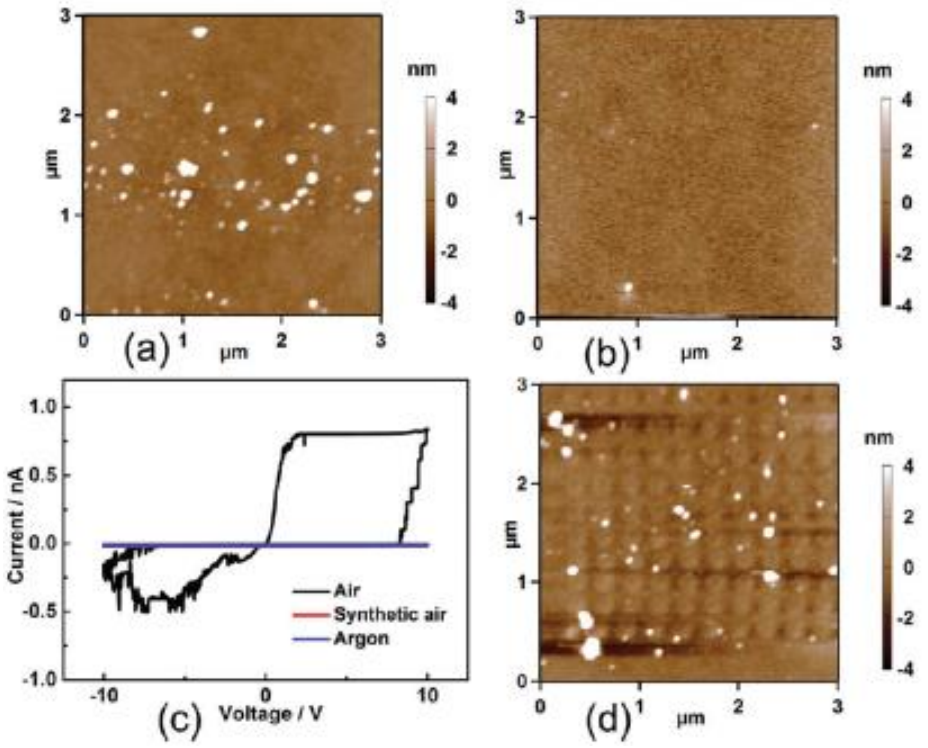

Fig. 5 (a) and (b) Topographic images after measuring I–V curves in (a) argon gas and (b) synthetic air. (c) Averaged I–V curves obtain in argon gas and synthetic air, as well as the I–V curve acquired after reinjecting ambient air. (d) Corresponding topographic image after reinjecting ambient air.

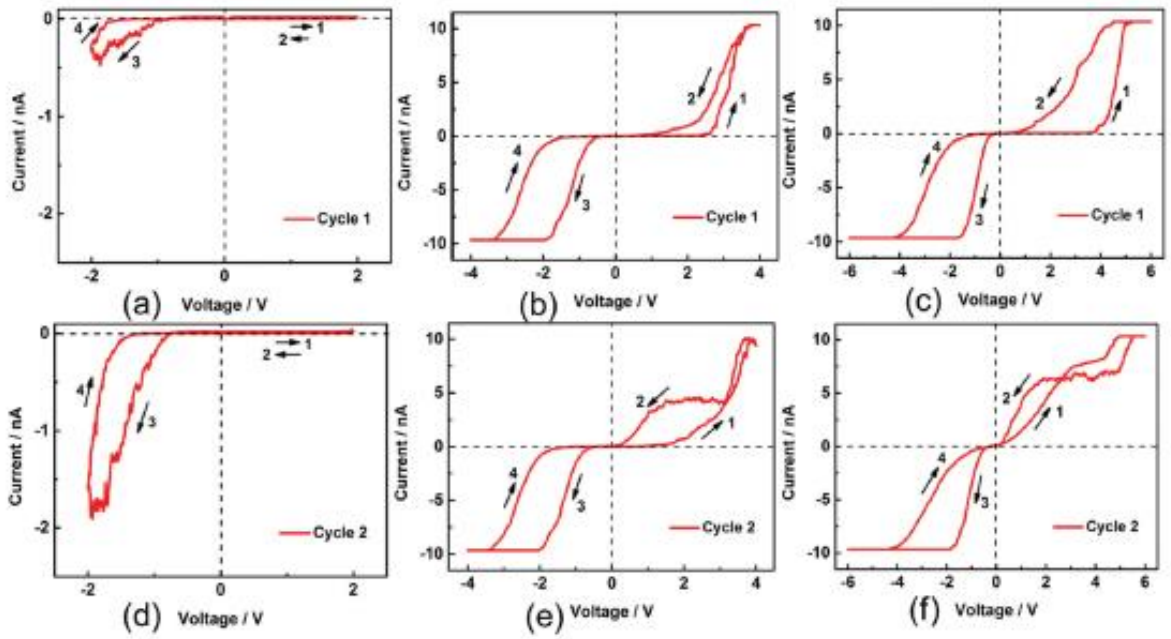

Fig. 6 (a)–(c) The first cycle of I–V curves with different bias amplitudes: (a) 2 V, (b) 4 V, and (c) 6 V. (d)–(f) The second cycle of I–V curves with different bias amplitudes: (d) 2 V, (e) 4 V, and (f) 6 V. The corresponding topography images are shown in Fig. 3.

3.4 Mechanisms underlying the electrochemically induced RS of TiO2 mediated by moisture

In the previous section, it has been demonstrated that the moisture mediated electrochemical phenomena underneath the SPM tip, including the reversible and irreversible electrochemical processes from the surface deformation (Fig. 2 and 3) and ESM responses (Fig. 4). Those electrochemical phenomena have been proved to be associated with the resistive switching behavior of the TiO_2 film. TiO_2 is a well-known electronic-ionic oxide with oxygen vacancies as the dominant mobile ions at room temperature.[79] Under an electrical field, the oxygen vacancies can be generated or annihilated and further migrate to form or disconnect the conductive filaments or change the interface between the oxide and the electrode, consequently causing the resistive switching of transition metal oxides.[19] Moreover, most SPM-based measurements including C-AFM, ESM used in this work are performed in the ambient air environment, where a moisture meniscus is inevitably present at the tip–sample junction. Considering the extreme small radius of the SPM tip (on the order of tens of nanometres), the concentrated electrical field underneath the SPM tip can be very large and likely to initiate a broad spectrum of electrochemical phenomena, i.e., the redox of the moisture and the oxygen vacancy,[47] as described in Fig. 7.

Under a negative sample bias, the annihilation of oxygen vacancies and the oxidation of the moisture can occur at the tip–sample junction, denoted as:

$$V_o^{\cdot\cdot} + 2e^- + O_2 \rightarrow O$$

$$H_2O + O_2 + 4e^- \rightarrow OH^-$$

where $V_o^{\cdot\cdot}$ is the oxygen vacancy and O is the oxygen in the lattice.

Whereas under a positive sample bias, the generation of oxygen vacancies and the reduction of the moisture can occur at the tip–sample junction, written as:

$$O \rightarrow O_2 + V_O^{\cdot\cdot} + 2e^-$$

and

$$2H_2O \rightarrow 4H^+ + O_2 + 4e^-$$

when the bias amplitude is small, the electrochemical phenomena can be limited without affecting the continuity of oxygen and cation sublattices, and those processes can contribute to the reversible electrochemical phenomena as well as the ESM responses shown in Fig. 4. As discussed in the Section 3.1, the interface based mechanism is supposed to explain the resistive switching behavior of the lateral TiO_2 cell. Therefore, the promoting effect of the reversible electrochemical processes on the resistive switching can be attributed to the accumulation of oxygen vacancies, protons and hydroxyl at the interface between TiO_2 and the SPM tip. When the bias amplitude is large, those electrochemical processes can be intensified so that the irreversible electrochemical phenomena can be activated to cause the deformation at the surface, for example, the surface damage as shown in Fig. 2 and 3. The surface deformation can originate from the phase transition induced by the oxygen vacancy, or the injection of proton and hydroxyl. The phase transition may change the conductivity of TiO_2 underneath the SPM tip and thus degrade the resistive switching behavior as shown in Fig. 6(c) and (f).

It should be noted that only the electrochemical processes underneath the SPM tip are discussed in this work. This can be due to several reasons: (i) C-AFM and ESM mainly measure the information in the vicinity of the tip–sample junction; (ii) the conduction bottleneck that is vital to resistive switching commonly resides at the tip/oxide interface due to the extremely small contact area compared with the Ag/oxide interface, and greater likelihood of being contaminated by oxidation, moisture, hydrocarbons and/or other particulates;[80] and (iii) the redox of Ag is possible when the bias is applied to the Ag electrode,[2,29,59,81] but the influence of the Ag redox on the resistive switching can be neglected if considering the large electrode distance, the ohmic contact between the Ag/TiO^2 interface, and the poor ion diffusion coefficient in TiO_2 due to the large size of Ag ions.

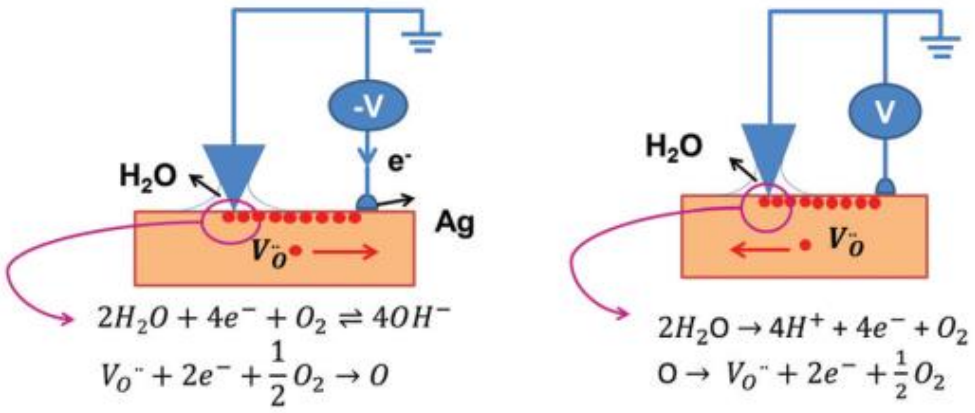

Fig. 7 The schematic of electrochemical reactions occurring at the tip–sample junction when applying (a) negative sample bias and (b) positive sample bias.

4. Summary and conclusions

In this work, a planar TiO_2 resistive switching cell is configured with the deposited Ag and the Pt-coated SPM tip as two electrodes, of which the electrode distance can be tuned by shifting the SPM tip over the sample surface to further control the mechanisms underlying resistive switching. In this work, the electrode distance is maintained on the millimeter-scale, and in this case, the interface based resistive switching dominates rather than the filament based mechanism underlying other resistive switching systems. Two advanced SPM techniques, C-AFM and ESM, are used to explore the responses of the TiO_2 resistive switching cell, the responses include the resistive switching performance, the ionic/electrochemical processes during the switching, and the effects of the electrochemical processes at different stages of the resistive switching performance. The electrochemical processes are found to strongly depend on the amplitude of the voltage used in the C-AFM measurement (specifically the I–V curve test). When the voltage is larger than 6 V, surface deformation can be found at locations where the I–V curve is measured, suggesting the irreversible electrochemical processes. When the voltage is less than 6 V, reversible electrochemical processes during the resistive switching are characterized by the ESM measurements which are correlated with C-AFM measurements at the same locations. The reversible and irreversible electrochemical processes are found to promote and suppress the resistive switching, respectively. Combined with a cell with environment control in which the desired air (argon gas or synthetic air) is introduced, C-AFM and ESM measurement results demonstrate that the

electrochemical processes need the participation of moisture. Thus, the accumulation of oxygen vacancies, protons, and hydroxyls in the Tip/TiO_2 interface can contribute to the promoting effect of the electrochemical processes; whereas the further accumulation and the injection of these ions into the TiO_2 lattice may lead to the suppressing effect. This work has demonstrated that moisture in the ambient air is a prerequisite for electrochemical processes and thus resistive switching of TiO_2. This is different from a previous report[78] in which oxygen was prerequisite due to the failure to decouple the effects of oxygen and moisture. The moisture effect on the resistive switching performance has been reported[82–84] recently but it is a discussion based on filament based resistive switching mechanisms, other than the interface based mechanism as shown in this work, which is also the reason for the reported moisture effect being different from this finding. In addition, the effects of electrochemical processes at different stages on resistive switching have been illustrated. All these results have provided a detailed understanding of the electrochemical processes during the resistive switching, also it can be extended for a better understanding of the electrochemical phenomena in various functional materials. The concentration of moisture adsorbed on the sample surface is proportional to the humidity of the environment. However, a quantitative study regarding the correlation between the moisture concentration (or the humidity) and the resistive switching performance is needed and is worthy of further exploration in the future.

Conflicts of interest

There are no conflicts to declare.

Acknowledgements

This work is supported by Ministry of Education (Singapore) through the National University of Singapore under the Academic Research Grant (AcRF) R-265-000-495-112. One of the authors (WHL) also thanks the postgraduate scholarship from the National University of Singapore.

References

1 T. C. Chang, K. C. Chang, T. M. Tsai, T. J. Chu and S. M. Sze, Mater. Today, 2016, 19, 254–264.

2 A. Sawa, Mater. Today, 2008, 11, 28–36.

3 A. Chanthbouala, A. Crassous, V. Garcia, K. Bouzehouane, S. Fusil, X. Moya, J. Allibe, B. Dlubak, J. Grollier, S. Xavier, C. Deranlot, A. Moshar, R. Proksch, N. D. Mathur, M. Bibes and A. Barthelemy, Nat. Nanotechnol., 2012, 7, 101–104.

4 A. Chernyshov, M. Overby, X. Y. Liu, J. K. Furdyna, Y. Lyanda-Geller and L. P. Rokhinson, Nat. Phys., 2009, 5, 656–659.

5 V. Garcia and M. Bibes, Nat. Commun., 2014, 5, 4289.

6 S. T. Han, Y. Zhou and V. A. L. Roy, Adv. Mater., 2013, 25, 5425–5449.

7 J. Hegedus and S. R. Elliott, Nat. Mater., 2008, 7, 399–405.

8 D. S. Jeong, R. Thomas, R. S. Katiyar, J. F. Scott, H. Kohlstedt, A. Petraru and C. S. Hwang, Rep. Prog. Phys., 2012, 75, 076502.

9 D. Pantel, S. Goetze, D. Hesse and M. Alexe, Nat. Mater., 2012, 11, 289–293.

10 T. Siegrist, P. Jost, H. Volker, M. Woda, P. Merkelbach, C. Schlockermann and M. Wuttig, Nat. Mater., 2011, 10, 202–208.

11 R. E. Simpson, P. Fons, A. V. Kolobov, T. Fukaya, M. Krbal, T. Yagi and J. Tominaga, Nat. Nanotechnol., 2011, 6, 501–505.

12 Z. Wen, C. Li, D. Wu, A. D. Li and N. B. Ming, Nat. Mater., 2013, 12, 617–621.

13 H. Akinaga and H. Shima, Proc. IEEE, 2010, 98, 2237–2251.

14 D. Lee, H. Choi, H. Sim, D. Choi, H. Hwang, M. J. Lee, S. A. Seo and I. K. Yoo, IEEE Electron Device Lett., 2005, 26, 719–721.

15 Q. Liu, S. B. Long, W. Wang, Q. Y. Zuo, S. Zhang, J. N. Chen and M. Liu, IEEE Electron Device Lett., 2009, 30, 1335–1337.

16 U. Russo, D. Ielmini, C. Cagli and A. L. Lacaita, IEEE Trans. Electron Devices, 2009, 56, 186–192.

17 K. Nagashima, T. Yanagida, K. Oka, M. Taniguchi, T. Kawai, J. S. Kim and B. H. Park, Nano Lett., 2010, 10, 1359–1363.

18 P. Hu, X. Y. Li, J. Q. Lu, M. Yang, Q. B. Lv and S. W. Li, Phys. Lett. A, 2011, 375, 1898–1902.

19 K. M. Kim, D. S. Jeong and C. S. Hwang, Nanotechnology, 2011, 22, 254002.

20 M. Son, J. Lee, J. Park, J. Shin, G. Choi, S. Jung, W. Lee, S. Kim, S. Park and H. Hwang, IEEE Electron Device Lett., 2011, 32, 1579–1581.

21 G. S. Park, Y. B. Kim, S. Y. Park, X. S. Li, S. Heo, M. J. Lee, M. Chang, J. H. Kwon, M. Kim, U. I. Chung, R. Dittmann, R. Waser and K. Kim, Nat. Commun., 2013, 4, 2382.

22 S. Zou, P. Xu and M. C. Hamilton, Electron. Lett., 2013, 49, 829–830.

23 F. Pan, S. Gao, C. Chen, C. Song and F. Zeng, Mater. Sci. Eng., R, 2014, 83, 1–59.

24 S. Tsui, A. Baikalov, J. Cmaidalka, Y. Y. Sun, Y. Q. Wang, Y. Y. Yue, C. W. Chu, L. Chen and A. J. Jacobson, Appl. Phys. Lett., 2004, 85, 317–319.

25 M. Janousch, G. I. Meijer, U. Staub, B. Delley, S. F. Karg and B. P. Andreasson, Adv. Mater., 2007, 19, 2232–2235.

26 R. Fors, S. I. Khartsev and A. M. Grishin, Phys. Rev. B, 2005, 71, 045305.

27 A. Sawa, T. Fujii, M. Kawasaki and Y. Tokura, Jpn. J. Appl. Phys., Part 2, 2005, 44, L1241–L1243.

28 J. J. Yang, M. D. Pickett, X. M. Li, D. A. A. Ohlberg, D. R. Stewart and R. S. Williams, Nat. Nanotechnol., 2008, 3, 429–433.

29 R. Waser and M. Aono, Nat. Mater., 2007, 6, 833–840.

30 R. Muenstermann, T. Menke, R. Dittmann and R. Waser, Adv. Mater., 2010, 22, 4819–4822.

31 K. P. Biju, X. J. Liu, S. Kim, S. Jung, J. Park and H. Hwang, Phys. Status Solidi RRL, 2011, 5, 89–91.

32 Y. M. Du, A. Kumar, H. Pan, K. Y. Zeng, S. J. Wang, P. Yang and A. T. S. Wee, AIP Adv., 2013, 3, 082107.

33 F. Gul and H. Efeoglu, Ceram. Int., 2017, 43, 10770–10775.

34 H. Y. Peng, L. Pu, J. C. Wu, D. Cha, J. H. Hong, W. N. Lin, Y. Y. Li, J. F. Ding, A. David, K. Li and T. Wu, APL Mater., 2013, 1, 052106.

35 C.-C. Hsu, W.-C. Ting and Y.-T. Chen, J. Alloys Compd., 2017, 691, 537–544.

36 R. K. Katiyar, Y. Sharma, D. G. B. Diestra, P. Misra, S. Kooriyattil, S. P. Pavunny, G. Morell, B. R. Weiner, J. F. Scott and R. S. Katiyar, AIP Adv., 2015, 5, 037109.

37 Z. M. Liao, C. Hou, Q. Zhao, D. S. Wang, Y. D. Li and D. P. Yu, Small, 2009, 5, 2377–2381.

38 K. Oka, T. Yanagida, K. Nagashima, T. Kawai, J. S. Kim and B. H. Park, J. Am. Chem. Soc., 2010, 132, 6634–6635.

39 W. Z. Wu and Z. L. Wang, Nano Lett., 2011, 11, 2779–2785.

40 Y. N. Chen, K. L. Pey, K. E. J. Goh, Z. Z. Lwin, P. K. Singh and S. Mahapatra, IEEE Trans. Electron Devices, 2010, 57, 3001–3005.

41 H. B. Zhao, H. L. Tu, F. Wei, X. Q. Zhang, Y. H. Xiong and J. Du, Rare Met., 2014, 33, 75–79.

42 J. Y. Son and Y. H. Shin, Appl. Phys. Lett., 2008, 92, 222106.

43 U. Celano, Y. Y. Chen, D. J. Wouters, G. Groeseneken, M. Jurczak and W. Vandervorst, Appl. Phys. Lett., 2013, 102, 121602.

44 U. Celano, L. Goux, R. Degraeve, A. Fantini, O. Richard, H. Bender, M. Jurczak and W. Vandervorst, Nano Lett., 2015, 15, 7970–7975.

45 J. Qi, M. Olmedo, J. J. Ren, N. Zhan, J. Z. Zhao, J. G. Zheng and J. L. Liu, ACS Nano, 2012, 6, 1051–1058.

46 J. X. Xiao, W. L. Ong, Z. M. Guo, G. W. Ho and K. Y. Zeng, ACS Appl. Mater. Interfaces, 2015, 7, 11412–11422.

47 S. V. Kalinin, S. Jesse, A. Tselev, A. P. Baddorf and N. Balke, ACS Nano, 2011, 5, 5683–5691.

48 S. Jesse, A. Kumar, T. M. Arruda, Y. Kim, S. V. Kalinin and F. Ciucci, MRS Bull., 2012, 37, 651–658.

49 S. Kalinin, N. Balke, S. Jesse, A. Tselev, A. Kumar, T. M. Arruda, S. L. Guo and R. Proksch, Mater. Today, 2011, 14, 548–558.

50 A. Kumar, F. Ciucci, A. N. Morozovska, S. V. Kalinin and S. Jesse, Nat. Chem., 2011, 3, 707–713.

51 A. Kumar, D. Leonard, S. Jesse, F. Ciucci, E. A. Eliseev, A. N. Morozovska, M. D. Biegalski, H. M. Christen, A. Tselev, E. Mutoro, E. J. Crumlin, D. Morgan, Y. Shao-Horn, A. Borisevich and S. V. Kalinin, ACS Nano, 2013, 7, 3808–3814.

52 S. Kalinin, A. Kumar, N. Balke, M. McCorkle, S. L. Guo, T. Arruda and S. Jesse, Adv. Mater. Processes, 2011, 169, 30–34.

53 A. N. Morozovska, E. A. Eliseev, N. Balke and S. V. Kalinin, J. Appl. Phys., 2010, 108, 053721.

54 Q. N. Chen, Y. Ou, F. Y. Ma and J. Y. Li, Appl. Phys. Lett., 2014, 104, 242907.

55 J. Li, J.-F. Li, Q. Yu, Q. N. Chen and S. Xie, J. Materiomic., 2015, 1, 3–21.

56 P. F. Yu, S. L. Hu and S. P. Shen, J. Appl. Phys., 2016, 120, 065102.

57 N. Balke, S. Jesse, Y. Kim, L. Adamczyk, A. Tselev, I. N. Ivanov, N. J. Dudney and S. V. Kalinin, Nano Lett., 2010, 10, 3420–3425.

58 N. Balke, S. Jesse, A. N. Morozovska, E. Eliseev, D. W. Chung, Y. Kim, L. Adamczyk, R. E. Garcia, N. Dudney and S. V. Kalinin, Nat. Nanotechnol., 2010, 5, 749–754.

59 R. Waser, R. Dittmann, G. Staikov and K. Szot, Adv. Mater., 2009, 21, 2632–2663.

60 D. B. Strukov, G. S. Snider, D. R. Stewart and R. S. Williams, Nature, 2008, 453, 80–83.

61 S. Williams, IEEE Spectrum, 2008, 45, 24–31.

62 D. H. Kwon, K. M. Kim, J. H. Jang, J. M. Jeon, M. H. Lee, G. H. Kim, X. S. Li, G. S. Park, B. Lee, S. Han, M. Kim and C. S. Hwang, Nat. Nanotechnol., 2010, 5, 148–153.

63 M. D. Pickett, D. B. Strukov, J. L. Borghetti, J. J. Yang, G. S. Snider, D. R. Stewart and R. S. Williams, J. Appl. Phys., 2009, 106, 074508.

64 K. Szot, M. Rogala, W. Speier, Z. Klusek, A. Besmehn and R. Waser, Nanotechnology, 2011, 22, 254001.

65 W. H. Lu, L. M. Wong, S. J. Wang and K. Y. Zeng, J. Electrochem. Soc., 2016, 163, E147–E153.

66 A. Gannepalli, D. G. Yablon, A. H. Tsou and R. Proksch, Nanotechnology, 2011, 22, 355705.

67 Q. N. Chen, Y. Y. Liu, Y. M. Liu, S. H. Xie, G. Z. Cao and J. Y. Li, Appl. Phys. Lett., 2012, 101, 063901.

68 B. J. Choi, D. S. Jeong, S. K. Kim, C. Rohde, S. Choi, J. H. Oh, H. J. Kim, C. S. Hwang, K. Szot, R. Waser, B. Reichenberg and S. Tiedke, J. Appl. Phys., 2005, 98, 033715.

69 C. Nauenheim, C. Kuegeler, A. Ruediger and R. Waser, Appl. Phys. Lett., 2010, 96, 122902.

70 J. Xiao, T. S. Herng, J. Ding and K. Zeng, J. Alloys Compd., 2017, 709, 535–541.

71 Y. Omura and Y. Kondo, J. Appl. Phys., 2013, 114, 043712.

72 A. Tsurumaki, H. Yamada and A. Sawa, Adv. Funct. Mater., 2012, 22, 1040–1047.

73 S. V. Kalinin, B. J. Rodriguez, S. Jesse, J. Shin, A. P. Baddorf, P. Gupta, H. Jain, D. B. Williams and A. Gruverman, Microsc. Microanal., 2006, 12, 206–220.

74 Y. Kim, E. Strelcov, I. R. Hwang, T. Choi, B. H. Park, S. Jesse and S. V. Kalinin, Sci. Rep., 2013, 3, 2924.

75 Y. Kim, A. N. Morozovska, A. Kumar, S. Jesse, E. A. Eliseev, F. Alibart, D. Strukov and S. V. Kalinin, ACS Nano, 2012, 6, 7026–7033.

76 A.N.Morozovska, E. A. Eliseev, G. S. Svechnikov and S.V.Kalinin, Phys. Rev. B, 2011, 84, 045402.

77 A. N. Morozovska, E. A. Eliseev, A. K. Tagantsev, S. L. Bravina, L. Q. Chen and S. V. Kalinin, Phys. Rev. B, 2011, 83, 235313.

78 Y. Kim, J. H. Jang, S. J. Park, S. Jesse, L. Donovan, A. Y. Borisevich, W. Lee and S. V. Kalinin, Nanotechnology, 2013, 24, 085702.

79 S. K. Kim, K. M. Kim, D. S. Jeong, W. Jeon, K. J. Yoon and C. S. Hwang, J. Mater. Res., 2013, 28, 313–325.

80 M. H. Lee, K. M. Kim, S. J. Song, S. H. Rha, J. Y. Seok, J. S. Jung, G. H. Kim, J. H. Yoon and C. S. Hwang, Appl. Phys. A: Mater. Sci. Process., 2011, 102, 827–834.

81 C. P. Hsiung, H. W. Liao, J. Y. Gan, T. B. Wu, J. C. Hwang, F. Chen and M. J. Tsai, ACS Nano, 2010, 4, 5414–5420.

82 T. Tsuruoka, K. Terabe, T. Hasegawa, I. Valov, R. Waser and M. Aono, Adv. Funct. Mater., 2012, 22, 70–77.

83 F. Messerschmitt, M. Kubicek and J. L. M. Rupp, Adv. Funct. Mater., 2015, 25, 5117–5125.

84 Q. N. Yin, C. Y. Wei, Y. D. Xia, B. Xu, J. Yin and Z. G. Liu, J. Phys. D: Appl. Phys., 2016, 49, 305101.